STABILITY ANALYSIS OF PERFECT AND IMPERFECT CYLINDERS USING MSC/NASTRAN LINEAR AND NONLINEAR BUCKLING

M. H. Schneider, Jr. and R. J. Feldes
McDonnell Douglas Aerospace
Huntington Beach, California

J. R. Halcomb and C. C. Hoff
The MacNeal-Schwendler Corporation
Los Angeles, California

ABSTRACT

The buckling behavior of cylindrical shells with and without initial geometric imperfections is investigated using a combined analytical and experimental approach. Seamless cylindrical plastic models were fabricated and tested under axial compression and external hydrostatic pressure as "perfect" cylinders. Upon completion of testing, the cylinders were reformed to a specified imperfection shape and re-tested. The thickness, modulus of elasticity, and geometric shape was measured for each cylinder. Analytical models were generated in MSC/PATRAN using measured imperfection shape and amplitude. Buckling loads were calculated in MSC/NASTRAN using the geometric nonlinear analysis provided in solution sequence SOL 106. These results were correlated to experiments and compared with results predicted by other computer codes. The finite element mesh spacing used in the correlation effort was based on the results of a mesh convergence study performed using the linear eigenvalue solution sequence SOL105. Good agreement between experimental results and other predictions was achieved.

INTRODUCTION

The load carrying capability of all structures is dependent on their geometry, material properties, and boundary conditions. The rather unique characteristic of shell structures, under compressive loading, is that their strength is very sensitive to initial geometric imperfections. The geometric imperfections referred to here are the deviations from circularity found in typical cylinders, and they are always present because of manufacturing tolerances. The presence of initial imperfections can greatly reduce the buckling load predicted for a shell of perfect geometry. To account for the effect of these imperfections, specifications and design criteria are used in the design of shells subjected to compressive loading. Design rules for commercial applications are given by the American Water Work Association (AWWA) (Ref. 1), American Petroleum Institute (API) (Ref. 2) or the American Society of Mechanical Engineers (ASME) (Ref. 3). The finite element method is also used extensively to predict shell buckling. Finite Element Analysis (FEA) has become the predominant design and analysis tool in the aerospace industry, where very large finite element models are built with the aid of preprocessors and solved by large general-purpose finite element codes. Typical finite element models are built assuming perfect cylindrical geometry and the results of the FEA are "knocked down" for the effect of imperfections. Design criteria for aerospace structures are given by NASA Space Vehicle Design Criteria for buckling given in SP8007 (Ref. 4), SP8019, (Ref. 5) and SP8032 (Ref. 6).

The present effort is part of a combined analytical and experimental program to investigate the effect of manufacturing induced imperfections on shell buckling loads. Currently, there is no method of relating manufacturing induced imperfections to shell buckling correlation (knockdown) factors. Such a method would be useful in defining the most efficient fabrication method and least expensive tooling, and would provide acceptance criteria based on the buckling failure mode, thereby providing guidance to engineering for evaluating discrepant hardware.

BACKGROUND & PROBLEM DEFINITION

Unlike plate structures, curved shells have little post-buckling capability. Therefore, buckling of the shell results in catastrophic failure. Consequently, worst case loads are used with design criteria that does not permit buckling. Figure 1a illustrates the axial compression buckling and post buckling behavior for a shell with an imperfection amplitude that is 30% of the shell thickness and has the same shape as the classical buckled shape. The buckling load is predicted to be 72% of the classical theoretical value; the post buckling load is only 22% of the classical value. As can be seen in Figure 1b, small imperfections lead to large reductions in the buckling load for cylinders under axial compression. The results from Budiansky (Ref. 7), the BOSOR 4 (Ref. 8) code and from Koiter (Ref. 9) are for the axisymmetric imperfection while those from Yamaki (Ref. 10) are for an asymmetric imperfection. For axial compression, the axisymmetric imperfection is the worst shape. Current design practice (Figure 1c) uses experimentally determined correlation factors. The correlation factor for axial compressive loading is related to the R/t ratio. A more useful parameter would be the imperfection amplitude to thickness ratio (w_o/t) as shown in Figure 1d. Here the theoretical results from Yamaki (Ref. 10), based on an asymmetric imperfection, are used to relate correlation factors corresponding to tolerances on shell geometry permitted by the aerospace industry and those permitted by the ASME Boiler and Pressure Vessel Code.

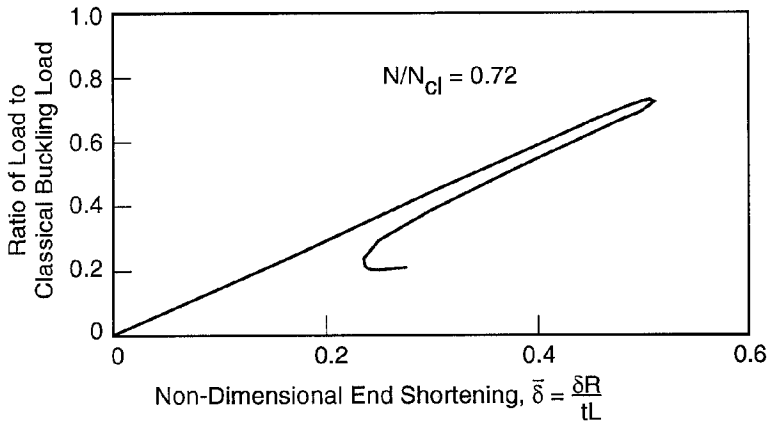

a. Curved elements have little post buckling load capability

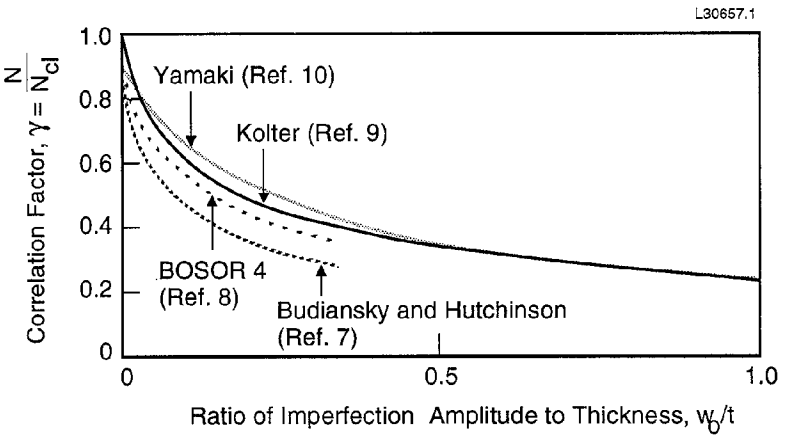

b. Small imperfections lead to a large reduction in theoretical buckling loads

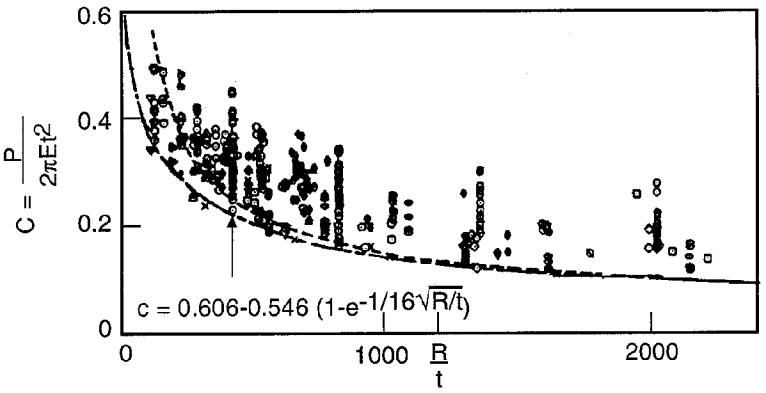

c. Current design practice uses experimentally determined correlation factors

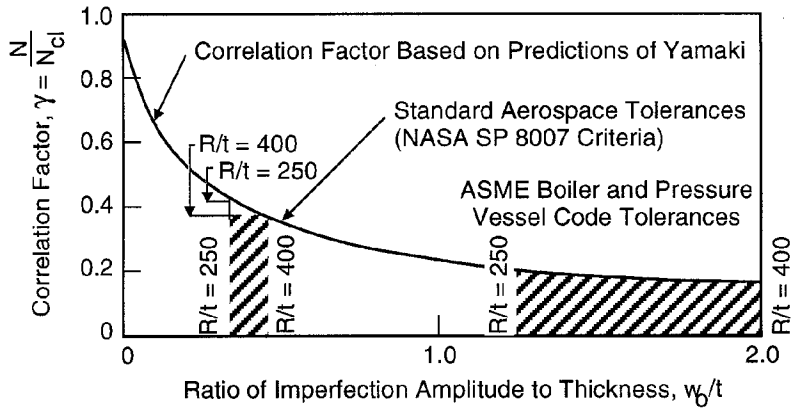

d. Need to relate correlation factors to manufacturing practice

Figure 1. Background

A significant difference in the correlation factors exists for these specifications. For an R/t=250 the correlation factor for aerospace tolerances is approximately twice that corresponding to the ASME boiler code. Since the required shell thickness is approximately a function of the square root of the correlation factor, a shell designed to the ASME boiler code tolerance will be 40% thicker (and heavier) than a shell designed to the aerospace tolerance.

The objective of this study is to develop a methodology for predicting the buckling of shells with initial imperfections. The long term goal is to develop design criteria through analyses and tests on scale models built with imperfections of known shape and amplitude.

PROGRAM PLAN

Figure 2 gives the flow diagram of the program plan for this study. Seamless cylindrical plastic models 15 inches in length and diameter with nominal wall thicknesses of 0.05 inch are fabricated from blow-molded bottle blanks. The thickness and shape of the cylinders are measured and the modulus of elasticity is determined by compression test on the cylinder. The "perfect" cylinder is then tested under axial compression and external hydrostatic pressure. Data for the "perfect" cylinder are correlated to predictions from the MSC/NASTRAN (Ref. 14), ABAQUS (Ref. 11), and BOSOR 4 (Ref. 8) computer codes.

Upon completion of this initial test series, the cylinder is reformed on a mandrel with the desired imperfection shape and amplitude. Only the shape and amplitude need to be measured since the thickness and modulus were previously determined. The same buckling test series is repeated and the results correlated to predictions. From this combined analytical and experimental program one can establish (1) a comparison between experiments for perfect and imperfect cylinders, (2) a correlation between experiments and analytical predictions, and (3) a comparison between analytical predictions.

TEST MODEL FABRICATION

The cylinders were thermal vacuum formed on collapsible mandrels (see Figure 3). The mandrel surface is machined to conform to a "perfect" cylindrical shape or an imperfection shape. One mandrel is required for each shape. In this initial portion of the program, two imperfection shapes were studied: 1) an axisymmetric shape corresponding to the worst-case imperfection for an axially loaded cylinder, and 2) an asymmetric shape corresponding to the critical buckling mode for an axially loaded cylinder. The asymmetric shape was obtained from the critical BOSOR 4 eigenvector which was translated into the Unigraphics drawing system and then to coding for the manufacturing operation.

After testing and verifying that the cylinders were near perfect, the cylinders were reformed on imperfect mandrels. The imperfection amplitude was selected as 30% ($w_o/t=0.3$) of the cylinder thickness because this amplitude along with worst-case imperfection spatial distributions produce knockdown factors for axial compression, external hydrostatic pressure, and shear buckling that are near those recommended by NASA SP8007 (Ref. 4).

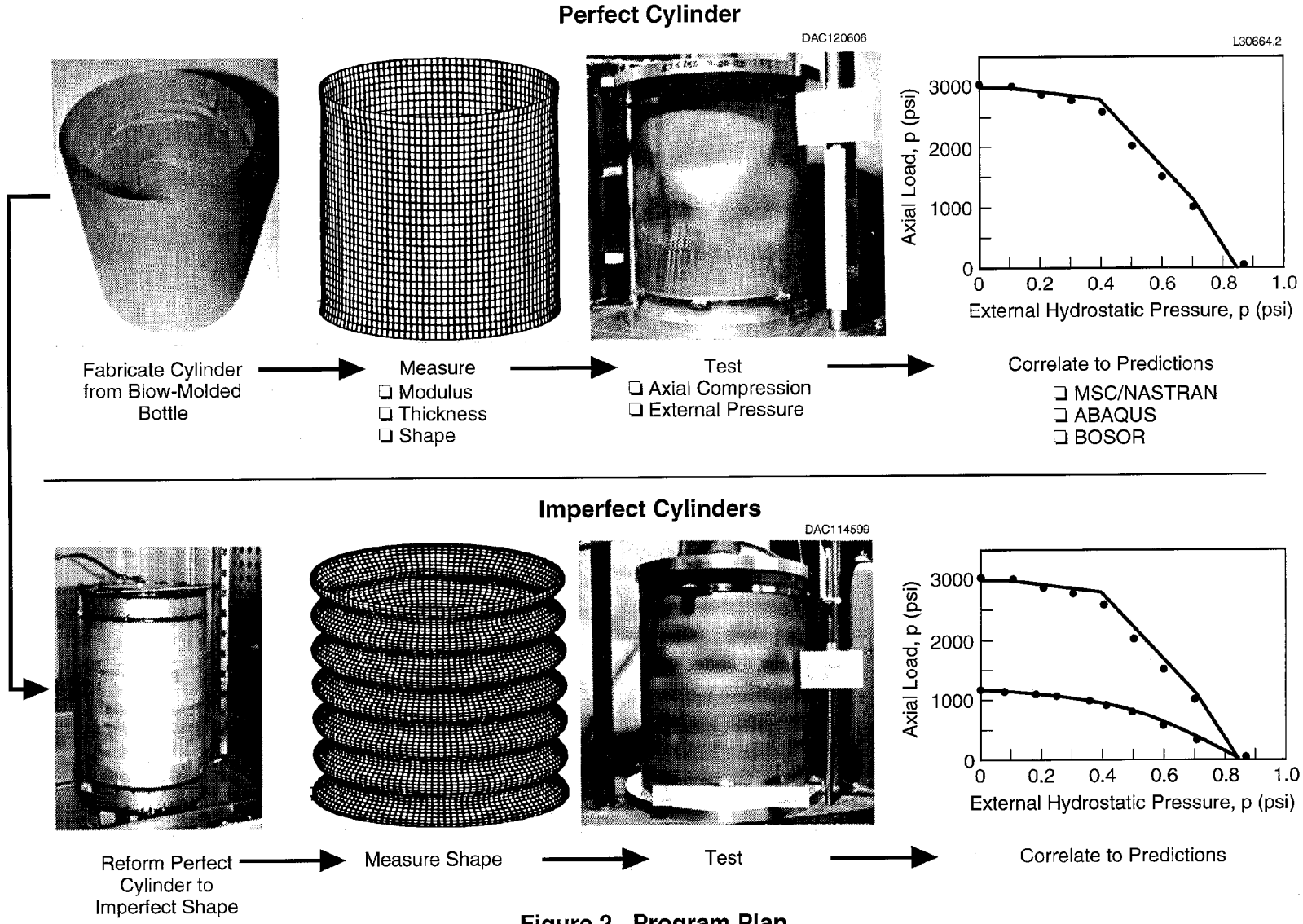

Figure 2. Program Plan

L30663

Mandrel

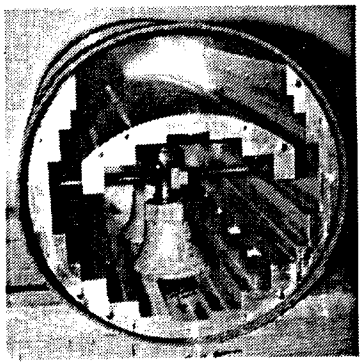

Collapsible Mandrel

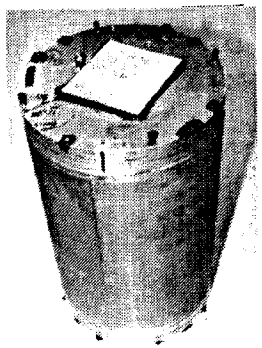

Machined to Shape

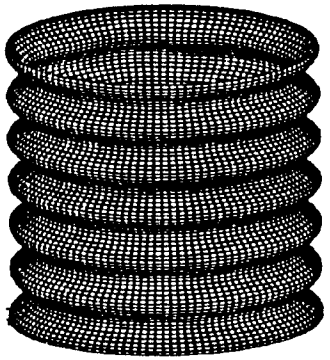

Lathe Operation for Perfect and Axisymmetric Shape

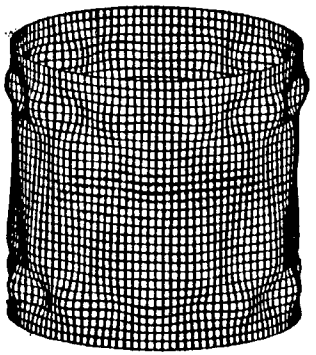

6 DOF Numerically Controlled Milling Machine for Asymmetric Shape

Test Cylinders

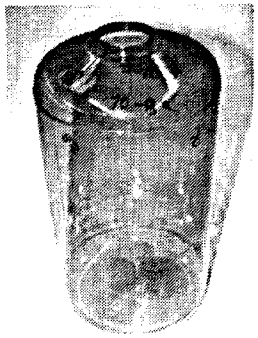

Blow Molded Bottle

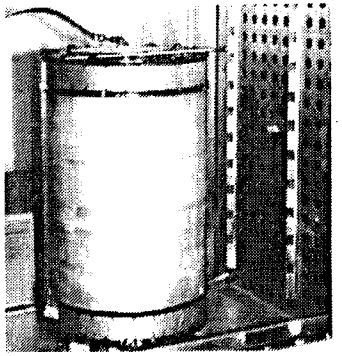

Thermal Vacuum Form on Perfect Mandrel

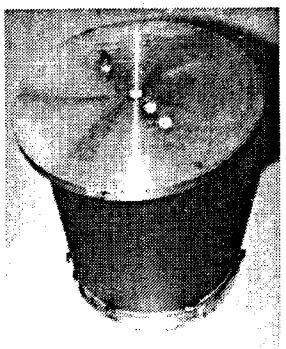

- ❑ Machine to Correct Thickness
  - ● Trim Ends
  - ● Attach End Plate

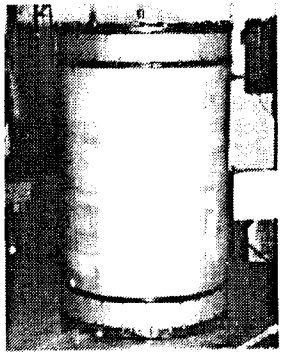

- ❑ Measure
- ❑ Test
- ❑ Reform on Imperfect Mandrel

FIGURE 3. Fabrication

Pretest analysis of the test cylinders with axisymmetric imperfections showed that the lowest buckling load occurred when the imperfection wave length corresponded to 13 axial half waves. At this wave length, a 30% imperfection still results in snap-through buckling, but a larger imperfection will result in axisymmetric collapse. The cylinder was predicted to buckle into 10 circumferential waves and this buckled shape was observed in the experiment.

EXPERIMENT DESCRIPTION

After fabrication of a cylinder was completed, the cylinder thickness was measured at 18 axial locations every 45° for a total of 144 locations. Thickness measurements were made to determine the average thickness to be used in the analytical predictions and also to establish that the maximum to minimum thickness difference was less than 0.003 inches. After the thickness of a cylinder was determined and found acceptable, the cylinder was fitted with aluminum load heads at each end, resulting in clamped boundary conditions. The modulus of elasticity was determined from load versus end-shortening data taken for each cylinder.

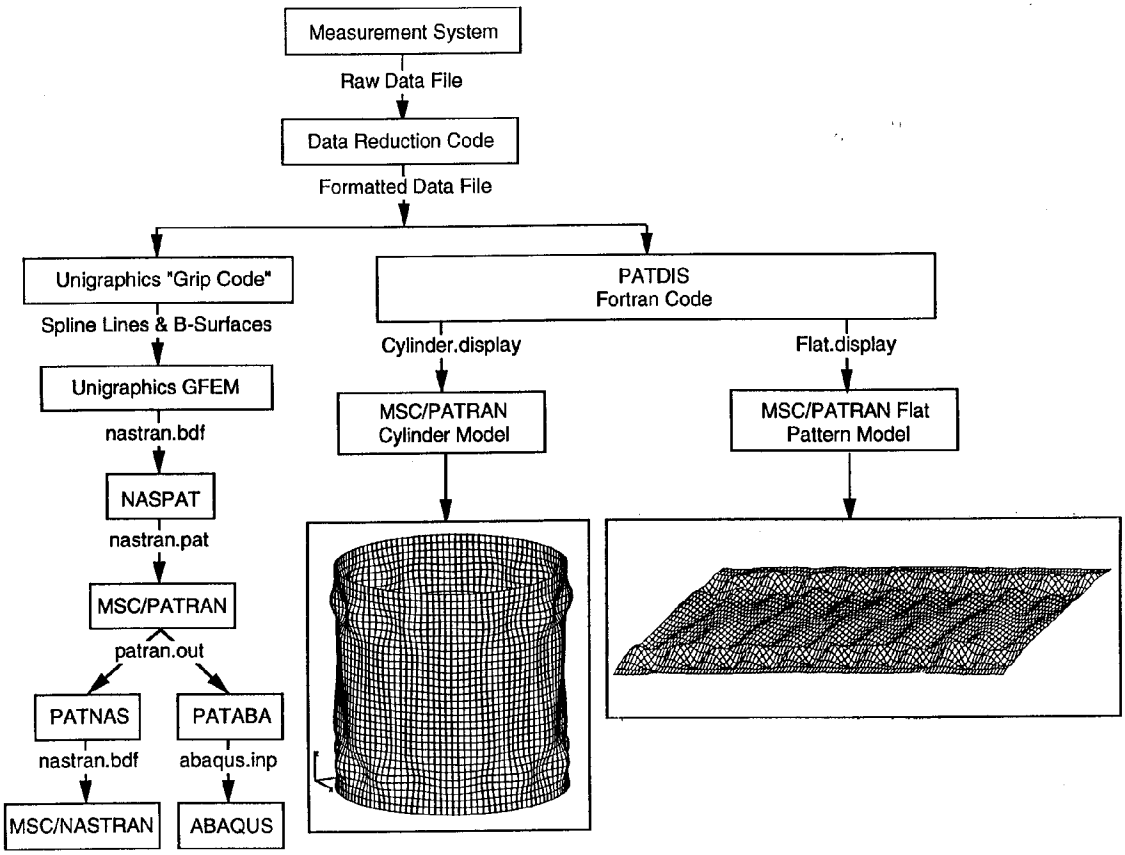

Figure 4. Flow Diagram for Processing Shape Data

In addition to thickness and modulus, shape data were needed to perform analytical predictions. Shape measurements were taken to characterize the imperfections and to verify the quality of the "perfect" cylinders. A Zeiss Measurement System was initially used because of its availability and because the data could be easily converted to analytical model mesh data or displayed. However, this system is restricted to small shapes (not much larger than the test cylinders) and consequently could not be used for typical full scale hardware. Therefore, a scanning measurement system was developed that, while only used in the model laboratory, would be adaptable to full scale hardware. Both systems produce the same quality and quantity of data at about the same costs.

Cylinder coordinates (R, θ, Z) were measured at 9600 locations. The data taken by either measurement system were processed by a data reduction program. From the formatted data file, the shape can be displayed in either a cylindrical coordinate system, or as a flat pattern development, and grid point model coordinates (R, θ, Z) can be created for a finite element mesh. Figure 4 shows the flow diagram of the process for displaying and translating measured data into the structural finite element model. MSC/PATRAN (Ref. 13) is a pre- and post-processor code that can be used with many general purpose finite element codes.

The shapes of the three tested cylinders are shown in Figure 5. These shapes are displayed as the deviation of the actual shape from an imaginary perfect cylinder. The radial deviation is shown as displacement from the perfect shape divided by thickness, w_o/t.

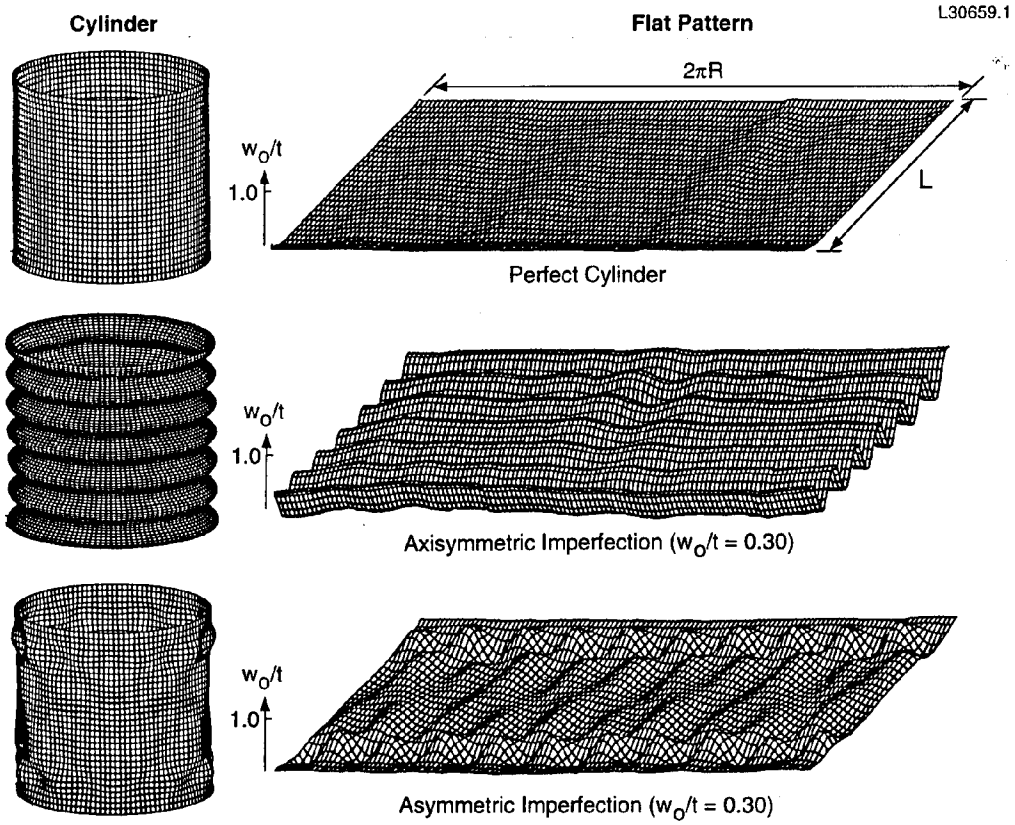

Figure 5. Measured Shapes

The cylinders were tested in a standard hydraulic test machine. A vacuum pump was used to evacuate the cylinder to produce external hydrostatic pressure. Load and end-shortening measurements were made and a video camera was used to record each test. Typically, several tests were conducted under the same loading conditions to verify results.

ANALYTICAL METHODS AND ANALYTICAL MODELS

The buckling load of the test models was predicted by seeking the lowest buckling eigenvalue from a nonlinear state of prebuckling stress. The presence of an initial imperfection requires the use of analysis methods that account for geometric nonlinearity. The experimental data were correlated to predictions made by the MSC/NASTRAN, ABAQUS, and BOSOR 4 computer codes.

MSC/NASTRAN and ABAQUS are large-scale, general-purpose computer codes that perform statics and dynamics by the finite element method. Because both the meridional and circumferential coordinates can be modeled, both axisymmetric and asymmetric imperfections can be accounted for.

The BOSOR 4 code performs stress, stability, and vibration analysis of complex branched shells of revolution by the finite difference method. The code is restricted to axisymmetric shapes and was used here to predict the buckling of "perfect" cylinders and those with axisymmetric imperfections. The buckle mode shape need not be restricted to the axisymmetric mode since BOSOR 4 will search for the lowest buckling load over a range of user supplied circumferential harmonics, or buckle wave shapes.

Figure 6 shows the mesh of four-node quadrilateral elements used in this study and provides some model statistics. Three 180° symmetry models were used with the MSC/NASTRAN and ABAQUS codes; one for "perfect" cylinders and one each for the two imperfect cylinders. All models had symmetry conditions imposed on the unloaded edges and clamped (all degrees of freedom fixed) conditions on the loaded edges representative of the test conditions. The full length of the cylinder was modeled to admit both symmetric and non-symmetric axial mode shapes.

The mesh spacing was chosen to adequately describe the axial and circumferential buckle wave lengths that were predicted. The mesh spacing in the axial direction, l_x, can be based on the classical half wave length for the axisymmetric mode, l_{cl}, determined by

$$l_{cl} = \frac{\pi}{\sqrt{2}\sqrt[4]{3(1-\mu^2)}}\sqrt{Rt} \qquad (1)$$

where R is the radius of curvature, t is the cylinder thickness, and μ is the Poisson's ratio. A typical rule of thumb is to have at least four elements per half-wave. The circumferential mesh is determined by the requirement to describe the circumferential half wave length. The circumferential mesh spacing should be less than 5° of arc to adequately model the curved surface with flat plate elements. Additionally, the aspect ratio of the flat elements should not exceed four.

A finer mesh is required for the imperfect cylinder model because, in addition to meeting the above criteria, the mesh must adequately model the imperfection shape mapped onto the mesh by the coordinate measuring system. The larger imperfect shape mesh with 24,015 active degrees-of-freedom (DOF) is considerably more computationally expensive than the smaller perfect shell mesh with 13,845 DOF.

MSC/NASTRAN and ABAQUS **BOSOR 4**

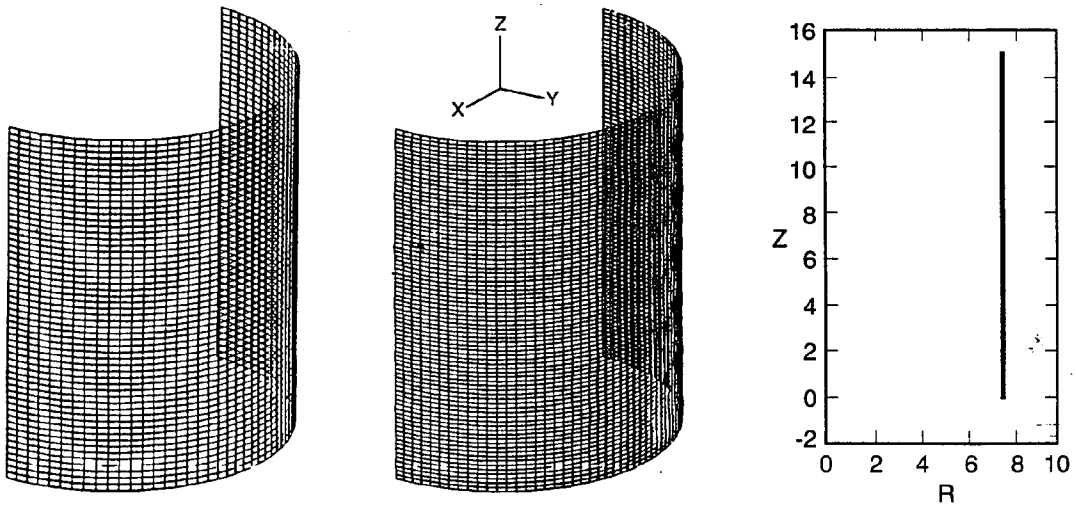

Perfect Cylinder
2,800 Elements
56 Elements Z-Direction
50 Elements Circumferential
13,845 Degrees of Freedom

Imperfect Cylinder
4,800 Elements
80 Elements Z-Direction
60 Elements Circumferential
24,015 Degrees of Freedom

400 Mesh Points

4 Segments

Figure 6. Analytical Model Mesh

Mesh Convergence Study in MSC/NASTRAN's Buckling Analysis

Prior to conducting a stability analysis with any finite element or finite difference code it is necessary to establish that the analytical model contains the appropriate mesh density to provide accurate predictions of the buckling load. MSC/NASTRAN linear buckling analysis (SOL105) was used to conduct a mesh convergence study similar to those performed previously for ABAQUS and BOSOR. The present study was performed by making five consecutive mesh refinements and computing the linear buckling load for the geometry and modulus of the perfect cylinder. The study was conducted using both versions V67.5 and V68 of MSC/NASTRAN. The results are plotted in Figure 7. In order to make this study applicable to a range of user problems, the computed buckling load has been normalized to the classical buckling load N_{cl}.

$$N_{cl} = \frac{1}{\sqrt{3(1-\mu^2)}} E \frac{t^2}{R} \tag{2}$$

The element spacing in the axial direction, l_x, has been normalized to the buckle half wave length in the axial direction for the axisymmetric mode, l_{cl}, given by equation (1).

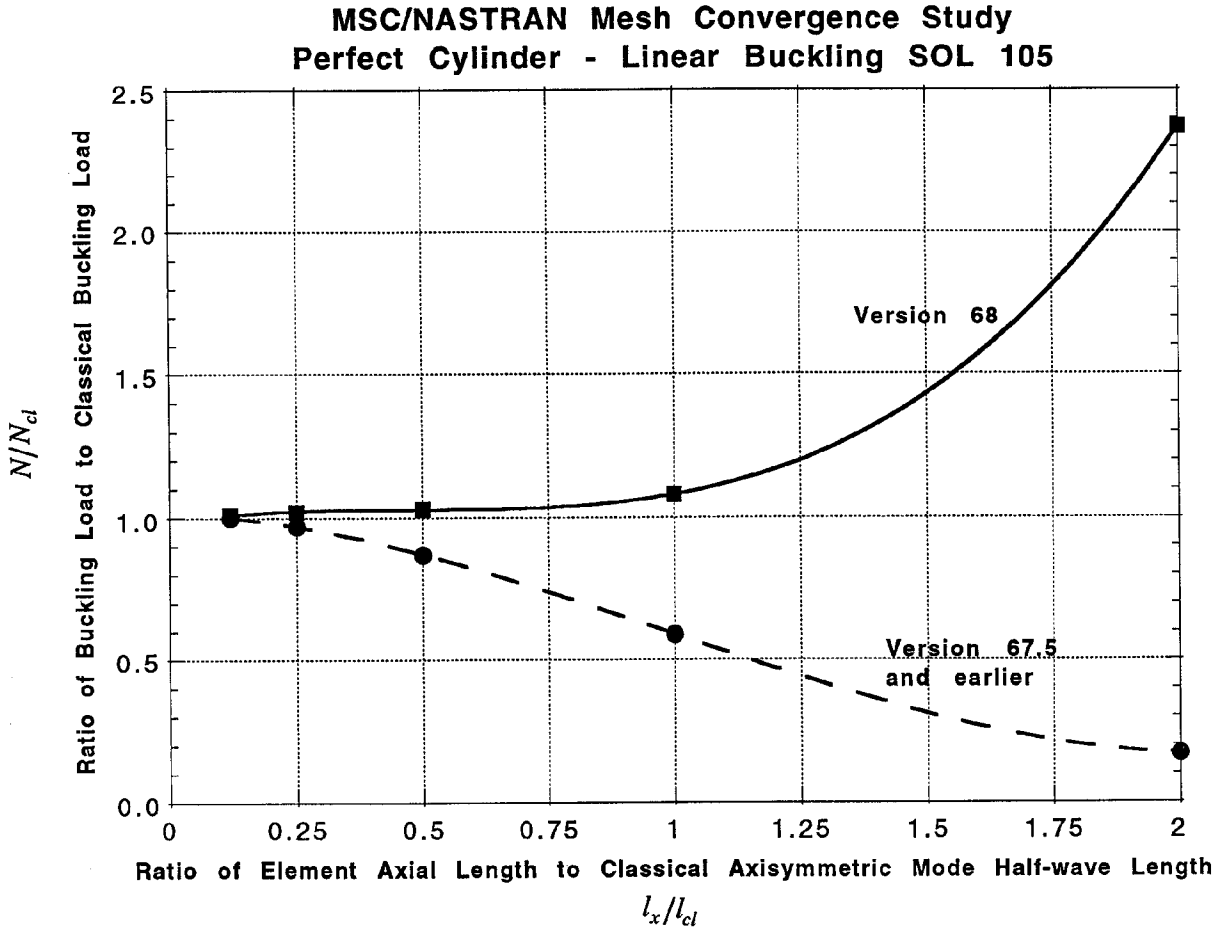

Figure 7 Mesh Convergence Study in MSC/NASTRAN

The results of this study show that buckling loads determined in V68 converge from above, with the buckling load decreasing as the mesh density is increased. This stiff-side convergence is what is typically expected from the linear and nonlinear finite element buckling analysis of shells. The results from V67.5 (and older versions) show convergence from below; as the mesh density increases the buckling load increases. The results of V68 and earlier versions differ because the stiffness matrix has been improved in V68. In MSC/NASTRAN, the tangent stiffness matrix is the sum of the linear stiffness and the differential (or geometric) stiffness matrices. In earlier versions of MSC/NASTRAN, the differential stiffness matrix had higher order bending terms which caused the convergence from below, and also resulted in the occurrence of spurious modes for thin shells. In V68, the higher order bending terms in the differential stiffness matrix have been eliminated; additional terms have also been added to account for large rotation effects.

MSC/NASTRAN Analysis Procedure

Two kinds of buckling analysis are available in MSC/NASTRAN. Linear buckling analysis is based on small deformations and linear material. The solution sequence for linear buckling is SOL 105. In nonlinear buckling analysis, geometric nonlinear effects and nonlinear materials are considered. Nonlinear buckling analysis is part of the nonlinear static solution sequence SOL 106. For this paper, SOL 106 was used for the buckling analysis because nonlinear geometric effects are important. SOL 105 was used only to demonstrate the convergence behavior described above and to compare to the results of the nonlinear analysis.

The nonlinear buckling analysis using SOL 106 in MSC/NASTRAN is performed using two sequential analysis runs -- a nonlinear statics analysis to establish the pre buckled state and the approximate instability load, followed by a second run to calculate the eigenvalue and eigenvector (the buckling load and mode shape). An optional third run seeking post-buckling behavior may be performed using the arc-length method in SOL 106. The analysis procedures are outlined below.

The linear and nonlinear buckling analyses in MSC/NASTRAN do not include follower force effects in the stiffness matrix. The calculated buckling loads are either too high or too low, depending on whether the follower forces destabilize or stabilize the structure. For shell structures, the follower force effect is important when buckling occurs with few circumferential waves. A cylinder subjected to external pressure will buckle into N waves in the circumferential direction and the buckling load will be over-predicted by the ratio of $N^2/(N^2-1)$. For most shells that buckle into many circumferential waves, (N=6 in this study) the error is negligible.

Linear Buckling Analysis in SOL 105

Linear buckling analysis is done in two subcases. In the first subcase the static load is applied and in the second subcase, a METHOD case control entry referencing an EIGB or EIGRL bulk data entry is used to activate the eigenvalue analysis. The buckling loads from the linear analysis are sometimes higher than the true buckling loads because geometric nonlinear effects, which are often important, are not included. However, the linear buckling load is a good estimate of the true buckling load if nonlinear effects are small, and is a useful value in determining the load steps for a nonlinear buckling analysis in which nonlinear effects are important.

Nonlinear Buckling Analysis in SOL 106

Initial Run The first SOL 106 run is a regular nonlinear static analysis, which for efficiency is usually run in two subcases. In the first subcase, a load is specified which is well below the expected buckling load. Nonlinear effects at these load levels are generally small, and large load increments can be specified along with default parameters on the NLPARM Bulk Data Entry. (See Ref. 14 for a detailed description of the NLPARM entry.) The default solution strategy is a modified Newton with the BFGS method and automatic bisection of load increments. The expected buckling load required for this solution may be obtained by first performing a linear eigenvalue analysis (SOL 105) or calculating the value from available closed form solutions.

In the second subcase, a maximum load above the expected buckling load is specified and small load increments are used. The results of each load step must be saved on the database for restart by setting the parameter INTOUT=YES on the NLPARM bulk data entry. The full Newton method is recommended which is also selected on the NLPARM bulk data entry by setting METHOD=ITER and KSTEP=1. As the solution proceeds through each small load step, a load will be reached where a negative factor diagonal occurs in the stiffness matrix. The negative term indicates the presence of the first eigenvalue, or instability point. The run may diverge after the stability point is passed. Care must be exercised to establish that the lack of convergence is induced by a stability limit and not due to poor convergence of the static solution resulting from too large a load step. There is no simple rule for determining load step size for the second subcase since the value will be problem dependent. When the eigenvalues are closely spaced, as with compression buckling of cylinders, a very small load step like 1% of the buckling load may be required. In other cases a value of 10% may be sufficient. Several trial runs may be required.

Restart Run The actual nonlinear buckling analysis is performed in a second SOL 106 run made by restarting from the initial run. The restart is made at a load that is two steps below the load step at which a negative factor diagonal was first detected in the nonlinear static analysis. The user provides the restart point using LOOPID and SUBID values on PARAM bulk data entries, where LOOPID is the load step identifier of the previous nonlinear static analysis and SUBID is the sequential subcase number of a new subcase.

Two load steps are applied in the new subcase to reach the critical point. The full Newton method must be used to get the true tangent stiffness matrices. The full Newton method is selected on the NLPARM card with METHOD=ITER and KSTEP=1.

Based on the two load steps, an eigenvalue analysis is executed to obtain the nonlinear buckling load and mode. The buckling analysis is requested using the PARAM,BUCKLE,1 bulk data statement. A METHOD Case Control Entry referencing an EIGB or EIGRL bulk data entry is required to activate the eigenvalue analysis.

Nonlinear Static Analysis with the Arc-Length Method in SOL 106

A third SOL 106 run may be made to check the calculated buckling load and to investigate the post-buckling behavior of the structure by using the arc-length method to go beyond the buckling point.

The solution is again restarted from the initial job at a load two steps below the load step with a negative factor diagonal (the same load step used for the nonlinear buckling analysis described above). A new subcase is introduced with small load steps on the NLPARM bulk data entry. In addition, the arc-length method is requested with the NLPCI bulk data entry. Default values on the NLPARM and NLPCI entries are recommended. The load in the new subcase must be above the buckling

load to ensure that the arc-length solution continues beyond the buckling point. The run will most likely diverge in the post-buckling branch unless the structure has a stable branch in that region. The buckling load is either the load at which the first negative term occurs on the factor diagonal or is the maximum of the load-deflection curve. The accuracy depends on the size of the arc-length around the stability point. When buckling is a bifurcation point, the most common situation for shells, the maximum of the load-deflection curve cannot be used to determine the initial buckling load.

RESULTS DISCUSSION

Axial Compression

Excellent agreement between theory and experiment for axial compression has been demonstrated. Table 1 gives analytical and experimental results for "perfect" and imperfect cylinders under axial compression loading.

TABLE 1. - Excellent Agreement Between Theory and Experiment Has Been Demonstrated for Axial Compression

Test Specimen Description	Experimental Results (lb)	Theory (lb) (% deviation)		
		MSC/NASTRAN Version 68	ABAQUS Version 4.8	BOSOR 4
Perfect cylinders				
S/N 81	3059	3165 (+3.5)	3085 (+0.8)	3046 (-0.4)
S/N 97	3015	3135 (+4.0)	3006 (-0.3)	3010 (-0.2)
S/N 78	3045	3100 (+1.8)	2936 (-3.6)	2960 (-2.8)
Imperfect cylinders				
Axisymmetric imperfection (w_o/t = 0.30 S/N 97)	1183	1239 (+4.7)	1235 (+4.4)	1181 (-0.2)
Asymmetric imperfection (w_o/t = 0.30 S/N 78)	1656	1716 (+3.6)	1658 (+0.1)	not applicable

Maximum deviation of theory and experiment was 4.7%. As predicted, the axisymmetric imperfection results in the greatest reduction in buckling load. Referring to Table 1, the buckling load resulting from an axisymmetric imperfection is (1183/3015)(100) = 39.2% that of the perfect cylinder based on a comparison of experimental data and is predicted to be 39.5% by MSC/NASTRAN, 41.1% by ABAQUS, and 39.2% by BOSOR 4. Similar results for the asymmetric imperfection are 54.4% by experiment, 55.4% by MSC/NASTRAN, and 56.5% by ABAQUS predictions.

External Hydrostatic Pressure

Excellent agreement between theory and experiment for external hydrostatic pressure has also been demonstrated (see Table 2). Maximum discrepancy between theory and experiment was 10.9%.

The imperfection shapes studied so far are those that are worst case for axial compressive loading. These imperfection shapes do not significantly reduce the buckling load under hydrostatic pressure. Experimental results for hydrostatic pressure show that the axisymmetric imperfection reduces the buckling pressure of the "perfect" cylinder by 1.5%. By comparison, MSC/NASTRAN predicts a 7.3% increase, ABAQUS a 1.7% increase, and BOSOR 4 a 3.1% increase. The asymmetric imperfection results in a reduction of 6.4% in buckling pressure based on experimental data, while MSC/NASTRAN predicts a 2.9% decrease.

TABLE 2. - Excellent Agreement Between Theory and Experiment Has Been Demonstrated for External Hydrostatic Pressure

Test Specimen Description	Experimental Results (psi)	Theory (psi) (% deviation)		
		MSC/NASTRAN Version 68	ABAQUS Version 4.8	BOSOR 4
Perfect cylinders				
S/N 81	0.870	0.900 (+3.4)	0.880 (+1.1)	0.851 (-2.2)
S/N 97	No experiment	0.885	0.863	0.834
Imperfect cylinders				
Axisymmetric imperfection (w_o/t = 0.30 S/N 97)	0.857	0.950 (+10.9)	0.878 (+2.5)	0.860 (+0.40)
Asymmetric imperfection (w_o/t = 0.30 S/N 78)	0.816	0.871 (+6.7)	Not calculated	Not applicable

SUMMARY AND CONCLUSIONS

This study on the effect of geometric imperfections on shell buckling loads illustrates that state of the art analysis tools can be used to accurately predict the complex nonlinear buckling behavior of imperfect shells, given the geometry of the imperfection. The ability of the lexan test models to be reconfigured and subjected to multiple loading conditions provided a comparison between experiments for perfect and imperfect cylinders using the same test model. The test data were correlated to MSC/NASTRAN, ABAQUS, and BOSOR 4 computer codes, and excellent agreement (within 4.7% for axial compression and within 10.9% for external hydrostatic pressure) was achieved.

Small amplitude axisymmetric imperfections of 30% of the shell thickness can result in a 60% reduction in buckling load. This illustrates how important imperfection shape and amplitude are in reducing the compressive load carrying capability of cylinders, and how important it is to minimize the effect of imperfections by controlling the fabrication and assembly process.

REFERENCES

1. Anon: Standard for Steel Tank-Standpipes, Reservoirs, and Elevated Tank for Water Storage. AWWA D-100-73, American Water Works Association, Denver, Colorado, 1973.
2. Anon: Bulletin on Stability Design of Cylindrical Shells, API Bulletin 2U (BUL 2U). First Edition. American Petroleum Institute, May 1987.
3. Anon: Boiler and Pressure Vessel Code. American Society of Mechanical Engineers, New York, New York, July 1989.
4. Anon: Buckling of Thin-Walled Circular Cylinders. NASA Space Vehicle Design Criteria (Structures), NASA SP-8007, revised 1968.
5. Anon: Buckling of Thin-Walled Truncated Cones. NASA Space Vehicle Design Criteria (Structures), NASA SP-8019, 1968.
6. Anon: Buckling of Thin-Walled Doubly Curved Shells. NASA Space Vehicle Design Criteria (Structures), NASA SP-8032, 1969.
7. Budiansky, B. and Hutchinson: Buckling of Circular Cylindrical Shells Under Axial Compression, in: Contribution to the Theory of Aircraft Structures pp. 239-259. Delft University Press, 1972.
8. Bushnell, D.: Analysis of Buckling and Vibration of Ring Stiffened, Segmented Shells of Revolution. International Journal of Solids and Structures, Vol. 6, No. 1, 1970 pp. 157-181.

9. Koiter, W. T.: On the Stability of Elastic Equilibrium (in Dutch) Thesis, Delft University 1945. Translation, AFFDL-TR-70-25, Air Force Flight Dynamic Laboratory, February 1970.
10. Yamaki, N.: Elastic Stability of Circular Cylindrical Shells. North-Holland Series in Applied Mathematics and Mechanics, Vol. 27, 1984.
11. Anon: ABAQUS Version 4.8 and 5.0. Hibbitt, Karlsson, and Sorensen, Inc. Pawtucket, Rhode Island 02860-4847.
12. Schneider, Jr., M.H., Snell, R.F., Tracy, J.J. and Powers, J.R.: Buckling and Vibration of Externally Pressurized Conical Shells with Continuous and Discontinuous Rings. AIAA Journal, Vol. 29, Number 9, September 1991, pp. 1515-1522.
13. Anon: MSC/PATRAN 2.5, The MacNeal Schwendler Corporation, PATRAN Division, Costa Mesa, California 92626.
14. Anon: MSC/NASTRAN Quick Reference Guide Version 68, The MacNeal Schwendler Corporation, Los Angeles, CA 90041 (1994)
15. Anon: MSC/NASTRAN Release Notes Version 68, The MacNeal Schwendler Corporation, Los Angeles, CA 90041 (1994)